ORIGINAL ARTICLE

Influences of boreal summer intraseasonal oscillation on tropical cyclone genesis and intensification over the Western North Pacific at the interannual timescale

Haoyu Zhou[1] · Pang-Chi Hsu[1] · Yitian Qian[1] · Wenjun Zhang[1]

Abstract

The climatological connection between tropical cyclones (TCs) and boreal summer intraseasonal oscillation (BSISO) over the western North Pacific (WNP) is known, but here we additionally find that the influences of May–October BSISO on TC genesis and intensification at the interannual timescale reveal distinctive regional features. The strengthened BSISO variability over the subtropical WNP (7.5°–27.5°N, 145°E–165°W) contributes positively to the basin-total TC genesis count, while the BSISO amplitude over the central-western equatorial Pacific (5°S–5°N, 140°E–160°W) is significantly correlated with the average intensity that TCs can reach. The physical processes causing the differences in TC behavior associated with interannual changes in BSISO are quantified from the viewpoint of eddy energetics. During summers with enhanced BSISO over the subtropical WNP, more TCs form there. Composite diagnostic analysis results for TC genesis days show that local synoptic eddies (or TC embryos) gain more kinetic energy to grow into TCs from both the seasonal-mean and BSISO anomalies via barotropic energy conversion. Eddy self-augmentation processes related to baroclinic conversion and eddy geopotential flux also aid the generation of TCs. During summers with enhanced central-western equatorial BSISO, TCs stay longer over the open ocean before they reach maximum intensity. Further diagnosis along the TC tracks shows that these eddies may grow faster (with a larger kinetic energy tendency) and reach a higher intensity with the help of enhanced barotropic and baroclinic energy conversion processes.

1 Introduction

Tropical cyclones (TCs) over the western North Pacific (WNP) are one of the most destructive types of natural disaster for coastal areas in populated Asia. An accurate prediction of TC activity is a critical but challenging issue for both the scientific and operational communities (Wu and Wang 2004; Zhan et al. 2012; Emanuel and Zhang 2017;

Qian et al. 2019; Trabing et al. 2023). Understanding the mechanisms responsible for the interannual variability of TC genesis and intensity is a key step towards improving the seasonal TC prediction skill (Chen et al. 2006; Tsuboi and Takemi 2014; Sobel et al. 2021; Cao et al. 2021).

The interannual variability of WNP TC activity has been commonly linked with the states of El Niño–Southern Oscillation (ENSO) because the ENSO-related sea surface temperature (SST) anomalies can induce various changes in large-scale conditions related to TC generation and intensification (Chan 1985; Wang and Chan 2002; Chia and Ropelewski 2002; Camargo et al. 2007; Cao et al. 2020). For example, TC genesis shows a southeastward displacement accompanied by a southeastward extension of the monsoon trough during warm ENSO years (Wang and Chan 2002; Camargo et al. 2007; Cao et al. 2020). Wang and Wu (2016) summarized the physical factors responsible for the

✉ Pang-Chi Hsu
  pangchi@nuist.edu.cn

[1] Key Laboratory of Meteorological Disaster, Ministry of Education, Joint International Research Laboratory of Climate and Environment Change, Collaborative Innovation Center on Forecast and Evaluation of Meteorological Disasters, Nanjing University of Information Science and Technology, Nanjing, China

southeastward shift of the mean location of WNP TC genesis as affected by ENSO, consisting of the effects of the SST anomaly (Li 1988) and changes in large-scale dynamic and thermodynamic conditions (Wang and Chan 2002; Chen et al. 2006; Camargo et al. 2007). Besides the TC genesis location, TC intensity is also known to vary with ENSO states. More intense TCs are observed during El Niño years, when TCs tend to generate in the southeastern WNP and stay longer over the ocean. During La Niña events, however, TCs form over the northwestern sector of the WNP and have a shorter period over the open ocean for intensification (Wang and Chan 2002; Camargo et al. 2007).

The changes in WNP synoptic-scale disturbances (or TC embryos) associated with ENSO are known to be a key factor influencing the TC activity at the interannual timescale (Hsu et al. 2009; Li et al. 2012; Wu et al. 2015). During El Niño years, the eastward-extended monsoon trough may interact with the westward-propagating mixed Rossby–gravity waves and their transition to tropical depression–type disturbances, which ultimately leads to more tropical cyclogenesis over the WNP (Wu et al. 2014). From an energetic standpoint, Hsu et al. (2009) diagnosed the source of synoptic-scale eddy kinetic energy (EKE) during the developing summer of El Niño years and found that the cyclonic and convergent flow anomalies associated with the southeastward extension of the monsoon trough are favorable for barotropic energy conversion from the background mean flow to eddies, thereby inducing increased EKE and TC genesis over the southeastern WNP.

The formation of TCs is modulated not only by the conditions of the seasonal mean state and synoptic eddy, but also by the boreal summer intraseasonal oscillation (BSISO), which is vigorous over the WNP (Maloney and Hartmann 2001; Hall et al. 2001; Hsu et al. 2011; Li and Zhou 2013; Zhao et al. 2015; Kikuchi 2021). During active phases of the BSISO, synoptic-scale disturbances are enhanced (Maloney and Hartmann 2001; Hsu et al. 2011; Zhou and Hsu 2023) and TCs occur more frequently and tend to cluster (Gao and Li 2011; Kikuchi 2021). The positive vorticity anomalies and increased moisture associated with the convective BSISO phases provide a favorable environment for TC genesis and growth (Li and Zhou 2013; Zhao et al. 2015). Besides, the BSISO also experiences interannual variability when the Pacific–Indian Ocean SST varies at the interannual timescale (Teng and Wang 2003; Lin and Li 2008; Wu and Cao 2017). During the developing stage of El Niño, BSISO activity over the western Pacific is enhanced, while it is weakened under a La Niña condition (Teng and Wang 2003; Chen et al. 2015, 2020). Thus, the combined phases of convective BSISO and El Niño events greatly increases the WNP cyclogenesis (Li and Zhou 2012; Tsuboi and Takemi 2014; Lin 2019).

Although the ENSO–TC, BSISO–TC and ENSO–BSISO connections have been identified and discussed in the previous studies as reviewed above, whether and how the interannual BSISO variability exerts significant influences on TC activity has not been fully addressed. Accordingly, the aim of this study was to identify the key processes resulting in the year-to-year variations of WNP TC genesis and intensification during summers with different BSISO features. It is worth noting that the interannual connection between various TC activities and BSISO characteristics may be influenced by background modulations from interannual climate modes, such as ENSO, the Pacific Meridional Mode (PMM), the Indian Ocean Dipole, and others, since we retain all these signals in our analysis. Section 2 introduces the data and methods utilized in this study. Section 3 presents and analyzes the results on the BSISO–TC connection at the interannual timescale. The physical processes through which TC genesis and intensification show distinct behaviors associated with interannual changes in BSISO are discussed in Sects. 4 and 5, respectively. Section 6 summarizes the main findings of this study.

2 Data and methods

2.1 Data

The data employed in this study included (1) daily outgoing longwave radiation (OLR) from the NOAA polar-orbiting satellites (Liebmann and Smith 1996) with a resolution of 2.5° longitude by 2.5° latitude; (2) daily zonal (u) and meridional (v) wind fields, vertical p-velocity (ω), geopotential (ϕ), and air temperature (T), from 1000 to 100 hPa, with a horizontal resolution of 1.5°×1.5°, from the ECMWF interim reanalysis (Dee et al. 2011); (3) six-hourly TC best-track data from the Joint Typhoon Warning Center. The analysis period is boreal summer (May to October) from 1979 to 2018, which is encompassed by all datasets and corresponds to the season with the most vigorous TC and BSISO activities over the WNP.

2.2 EKE budget equation

The EKE budget equation has been widely used to quantify the contribution of BSISO and seasonal mean flow to synoptic-scale eddies from the perspective of atmospheric energetic processes (Maloney and Hartmann 2001; Chen and Huang 2009; Hsu et al. 2011, 2017; Tsou et al. 2014). According to Tsou et al. (2014) and Hsu et al. (2017), the three-dimensional EKE budget equation can be formulated as follows:

$$\frac{\partial K'}{\partial t} = \underbrace{-V' \cdot (V'_3 \cdot \nabla_3)\,\bar{V}}_{CK_{M-E}} \underbrace{-V' \cdot \left[\left(V'_3 + V^*_3\right) \cdot \nabla_3\right] V^*}_{CK_{I-E}} \underbrace{-\nabla_3 \cdot (V'_3 \phi')}_{BG}$$
$$\underbrace{-\left[\left(\overline{V_3} + V^*_3 + V'_3\right)\right] \cdot \nabla_3 K'}_{BK} \underbrace{-\frac{R}{P} T'\omega'}_{CE} + D \qquad (1)$$

Here, a prime represents the synoptic-scale (< 10 days) variability, while an asterisk and overbar indicate the 10–90-day intraseasonal component and background mean flow (90-day and longer), respectively. The three timescale components are obtained by applying a Lanczos band-pass filter (Duchon 1979). K' is the EKE [$K' = (u'^2 + v'^2)/2$]; t is time; V is the horizontal velocity vector; ∇ is the horizontal gradient operator; the subscript "3" presents the three-dimensional components; φ is geopotential; T is temperature; ω is vertical velocity; P is pressure; R is the gas constant; and D represents all the sub-grid processes.

According to the EKE budget equation, the changes in EKE [i.e., the l.h.s of Eq. (1)] can be modulated by all terms on the r.h.s of Eq. (1). Terms CK_{M-E} and CK_{I-E} represent the barotropic energy conversions from background mean flow and BSISO to EKE, respectively. The formulae of CK_{M-E} and CK_{I-E} are written in Eq. (2) and Eq. (3), respectively, consisting of 6 and 12 individual terms as follows. Term BK represents the advection of EKE. These three terms (CK_{M-E}, CK_{I-E} and BK) involve the processes of scale interactions among mean flow, BSISO, and eddies. In contrast, term BG, which represents the effect of eddy geopotential flux, and term CE, which expresses the baroclinic energy conversion from the eddy available potential energy (EAPE) to EKE, are related to eddy–eddy interaction.

$$CK_{M-E} = -\left(u'u'\frac{\partial \bar{u}}{\partial x} + u'v'\frac{\partial \bar{u}}{\partial y} + u'\omega'\frac{\partial \bar{u}}{\partial p}\right.$$
$$\left. + v'u'\frac{\partial \bar{v}}{\partial x} + v'v'\frac{\partial \bar{v}}{\partial y} + v'\omega'\frac{\partial \bar{v}}{\partial p}\right) \qquad (2)$$

$$CK_{I-E} = -\left(u'u'\frac{\partial u^*}{\partial x} + u'v'\frac{\partial u^*}{\partial y} + u'\omega'\frac{\partial u^*}{\partial p}\right.$$
$$\left. + v'u'\frac{\partial v^*}{\partial x} + v'v'\frac{\partial v^*}{\partial y} + v'\omega'\frac{\partial v^*}{\partial p}\right)$$
$$-\left(u'u^*\frac{\partial u^*}{\partial x} + u'v^*\frac{\partial u^*}{\partial y} + u'\omega^*\frac{\partial u^*}{\partial p}\right.$$
$$\left. + v'u^*\frac{\partial v^*}{\partial x} + v'v^*\frac{\partial v^*}{\partial y} + v'\omega^*\frac{\partial v^*}{\partial p}\right) \qquad (3)$$

2.3 Definitions of TC activity

For better analyzing the interannual relationship between BSISO and TCs, the six-hourly best-track data were converted to daily averaged values. To exclude weak TC cases, such as tropical depressions, which lack intensification processes and exhibit short lifespans, we specifically include TCs with maximum sustained winds ≥ 34 knots for analysis in this study. In other words, our focus is solely on tropical storms and typhoons. To quantitatively measure the TC activities, the following metrics are defined and analyzed:

(1) According to previous studies (Wang and Chan 2002; Webster et al. 2005; Camargo and Polvani 2019), the date and location of TC formation are defined as the timing and longitude/latitude when the TC first reaches 34 knots, respectively.
(2) TC accumulated cyclone energy (ACE; Bell et al. 2000), which is defined as the sum of the square of the wind speed throughout the lifetime of a TC, is widely used to measure the overall TC activity. The ACE can be computed by considering all TC cases within the WNP basin during the summer season, referred to as the basin-total ACE (Zhang et al. 2016); it can also present the accumulated TC intensity at each grid point when illustrating the geographical distribution of ACE (Murakami et al. 2014).
(3) The sustained wind velocity is defined as the TC intensity; the maximum intensity of a TC is recorded when the sustained wind velocity reaches its maximum value during the TC's lifetime.
(4) The categories of TC refer to the Saffir–Simpson hurricane wind scale. A tropical storm (TS) is characterized with a lifetime wind speed between 34 and 64 knots, while intense typhoons are classified into categories 1–3 (lifetime wind speed between 64 and 112 knots) and categories 4–5 (lifetime wind speed greater than 113 knots).
(5) The TC intensifying period is defined as the days with a positive tendency of sustained wind speed at a 24-hour interval before the TC reaches its maximum intensity (Zhou et al. 2018).
(6) The duration of the TC's lifespan is calculated as the days for TCs to maintain the tropical storm intensity or stronger.
(7) The TC genesis potential index (GPI), proposed by Emanuel and Nolan (2004), describes the major processes determining TC genesis. Here, we use the modified version of the GPI (Murakami and Wang 2010) in which the vertical motion effect is incorporated into the original GPI formula, which is written as.

$$GPI = \left|10^5 \eta\right|^{\frac{3}{2}} \left(\frac{RH}{50}\right)^3 \left(\frac{V_{pot}}{70}\right)^3 (1 + 0.1 V_s)^{-2} \left(\frac{-\omega + 0.1}{0.1}\right) \qquad (4)$$

where η is the 850-hPa absolute vorticity (s^{-1}), RH is the 700-hPa relative humidity (%), V_{pot} is the TC maximum

potential intensity (MPI, m s^{-1}) (Emanuel 1995; Bister and Emanuel 1998), V_s is the magnitude of the vertical wind shear (m s^{-1}) between 850 and 200 hPa, and ω is the 500-hPa vertical p-velocity (Pa s^{-1}). To simplify the expression of Eq. (4), we use ζ, q, ψ, υ, and ω to present the effect of individual terms, as follows:

$$GPI = \zeta \cdot q \cdot \psi \cdot \upsilon \cdot \omega \tag{5}$$

To examine the BSISO-associated GPI variations, we compute the daily GPI based on the fields with the climatological annual cycle and BSISO components, referred to as *GPI**. The relative contributions of each term to *GPI** can be decomposed following the approach of Jiang et al. (2012), as follows:

Fig. 1 Interannual standard deviations of (**a**) BSISO amplitude (units: W m^{-2}), (**b**) frequency of TC genesis in each 1.5° grid box (units: number), and (**c**) TC maximum intensity (units: knots), over the WNP during boreal summer (May–October), 1979–2018. The BSISO amplitude in each summer is defined as the standard deviation of 10–90-day OLR during May–October. The frequency of TC genesis is computed by the numbers of TC that appear within the specific grid box when it reaches the intensity of 34 knots. TC max intensity is recorded as the maximum sustained wind speed of the TC when the maximum values occur

$$GPI^* = \bar{\zeta}\bar{q}\bar{\psi}\bar{\upsilon}\omega^* + \bar{\zeta}\bar{q}\bar{\psi}\bar{\omega}\upsilon^* + \bar{\zeta}\bar{q}\bar{\upsilon}\bar{\omega}\psi^* \\ + \bar{\zeta}\bar{\psi}\bar{\upsilon}\bar{\omega}q^* + \bar{q}\bar{\psi}\bar{\upsilon}\bar{\omega}\zeta^* + NL \tag{6}$$

,in which the overbar symbolizes the climatological seasonal-mean components, while the asterisk reflects the 10–90-day BSISO components. NL involves high-order variances of two or more terms related to perturbations (such as $\bar{\zeta}\bar{q}\bar{\psi}\upsilon^*\omega^*$ and $\bar{\zeta}\bar{q}\psi^*\upsilon^*\omega^*$). For our definition of *GPI**, there are a total of 26 terms in NL. Compared to terms with a single BSISO parameter [the first 5 terms on the r.h.s of Eq. (6)], each individual term of NL (e.g., terms $\bar{\psi}\bar{\upsilon}\bar{\omega}q^*\zeta^*$, $\bar{\upsilon}\bar{\omega}q^*\zeta^*\psi^*$, $\bar{\omega}q^*\zeta^*\psi^*\upsilon^*$) is much smaller, although their summation could be large. Considering the complexity and small amplitude of individual NL processes, we primarily focus on the impacts of single BSISO-related parameter on *GPI** to the first order.

2.4 TC removal approach

Previous studies documented that TCs themselves could contribute to the background states through up-scale feedback (Hsu et al. 2008). To more clearly examine and quantify the effects of background conditions on TCs, we conducted parallel analyses using data in which TCs had been artificially removed, employing the method proposed by Kurihara et al. (1995). As per Kurihara et al. (1995), the low-level (850-hPa) wind and other fields can be separated into a basic and a disturbance component using a smoothing operator. Subsequently, the TC center and radius are determined based on the tangential wind profile of the disturbance component. Within this TC domain, the disturbance components of any fields of interest are replaced by the corresponding smoothed components. Finally, the reconstructed fields, comprising solely smoothed components (without the disturbance components) for a TC domain, are added to the basic fields to obtain the TC-removed variables.

3 Interannual relationship between BSISO variability and TC activity

The interannual variations of BSISO and TC activity are represented by the standard deviations of 10–90-day BSISO amplitude (i.e., standard deviations of 10–90-day OLR) and TC genesis/intensity averaged in each grid cell during May–October of each year, respectively. In agreement with previous studies (Chia and Ropelewski 2002; Chen et al. 2006; Wu and Cao 2017; Wang and Wu 2020; Cao et al. 2021; Kikuchi 2021), we found that the BSISO amplitude, TC genesis counts, and TC intensity all reveal remarkable interannual variability over the WNP (Fig. 1). However, the regions with large variations at the interannual timescales
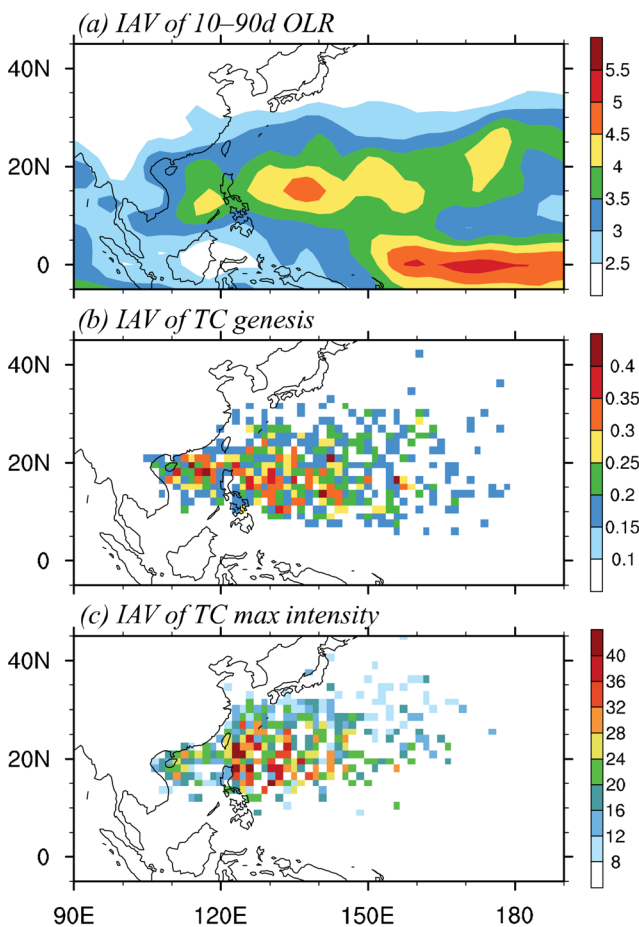
for BSISO and TC perturbations are slightly different. For the BSISO, it shows large variations at the interannual timescale over two areas. One is located in the central-western equatorial WNP; the other appears over the subtropical WNP (Fig. 1a). The TC genesis counts display the maximum interannual changes over the South China Sea–Philippine Sea area (Fig. 1b), while the TC maximum intensity varies interannually over the western portion of WNP (Fig. 1c).

To examine whether the year-to-year variations of TC activity are connected with the BSISO variability, we analyze the interannual correlations between various TC activity metrics and the BSISO. Figure 2a displays the correlation maps between the basin-total ACE index and the BSISO amplitude (standard deviations of 10–90-day OLR) in each grid cell based on the data of 1979–2018 summers (May–October). The result shows that the overall TC activity (ACE) is positively correlated with the BSISO over the southeastern WNP. This suggests that WNP-basin TC activity (defined by ACE) tends to be stronger during summers with enhanced BSISO over the southeastern WNP. Since the ACE is determined by the TC genesis count, intensity and lifetime duration, we repeated the correlation analysis for individual TC indices against the year-to-year BSISO amplitude to understand whether the regional BSISO changes show consistent effects on the interannual anomalies of TC genesis, intensity and lifespan (Fig. 2b–d). The results reveal that the key BSISO signals that modulate TC genesis and intensity/lifespan come from different areas. The BSISO amplitude over the subtropical WNP (7.5°–27.5°N, 145°E–165°W; blue box in Fig. 2b) is significantly correlated with the TC genesis count at the interannual timescale, implying that more TCs may be formed over the entire WNP basin when the BSISO intensifies over the subtropical

WNP. In contrast, the key regional BSISO affecting the basin-averaged TC maximum intensity and lifespan in each summer is observed over the central-western tropical and subtropical Pacific (5°S–17.5°N, 140°E–160°W) (Fig. 2c, d). To examine whether the tropical and subtropical BSISO signals both play an essential role in modulating TC intensity at the interannual timescale, we computed the correlation coefficients of yearly averaged TC intensity against time series of BSISO amplitude over the regions including (5°S–17.5°N, 140°E–160°W) and excluding the subtropical WNP (5°S–5°N, 140°E–160°W). The correlations for the former and latter cases are 0.38 and 0.42, respectively; both are statistically significant. This suggests that the interannual changes in TC intensity are predominantly regulated by equatorial BSISO amplitude (5°S–5°N, 140°E–160°W; purple box in Fig. 2c). Owing to the similarity between Fig. 2c and d, we suspect a linkage between the maximum TC intensity and TC lifespan duration, as discussed in previous studies derived from climatological-mean analysis (Wang and Chan 2002; Camargo et al. 2007). Our results further reveal that the WNP TCs may reach a higher intensity and have a longer duration during summers with vigorous BSISO variability over the central-western equatorial Pacific.

The analysis of Fig. 2 not only suggests a significant connection between the BSISO variability and WNP TC activity at the interannual timescale, but also discloses the different origins of BSISO variability (subtropical WNP vs. central-western equatorial Pacific) affecting the TC genesis and intensity. How the BSISO variability in different locations modulates TC behavior is a key question addressed in the following sections.

Fig. 2 (a) Correlation map between the yearly BSISO amplitude (standard deviations of 10–90-day OLR in summer) in each grid cell and the WNP basin-total ACE index (value per year) during May–October, 1979–2018. (b–d) Similar to (a) but for the correlations between the yearly BSISO amplitude in each grid cell and the WNP basin-total TC genesis count, averaged maximum TC intensity, and lifespan during each summer, respectively. Stippling denotes regions with a significant correlation coefficient at the 95% confidence level. The blue box in (b) and purple box in (c) mark the regions where the BSISO amplitude shows evident connections with WNP TC genesis counts and maximum intensity at the interannual timescale
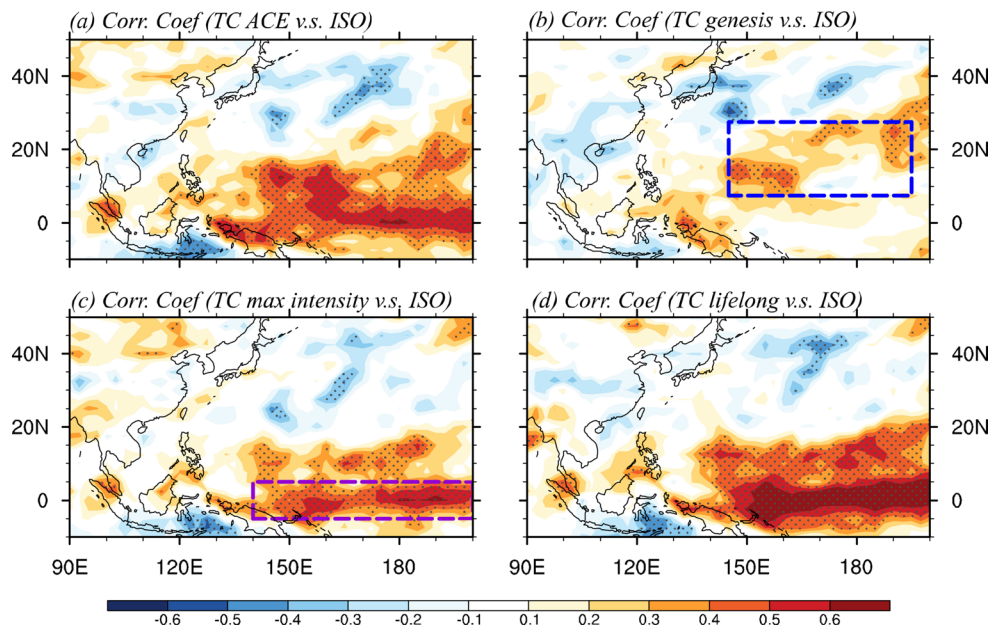

(a) Corr. Coef (TC ACE v.s. ISO)

(b) Corr. Coef (TC genesis v.s. ISO)

(c) Corr. Coef (TC max intensity v.s. ISO)

(d) Corr. Coef (TC lifelong v.s. ISO)

Fig. 3 Normalized amplitude of BSISO over the (**a**) sub-tropical WNP (7.5°–27.5°N, 145°E–165°W; blue box in Fig. 2b) and (**b**) central-western equatorial WNP (5°S–5°N, 140°E–160°W; purple box in Fig. 2c). Red characters in (**a**) and (**b**) denote the years with enhanced BSISO (greater than a standard deviation of normalized area-averaged BSISO amplitude) over the key region for increased TC 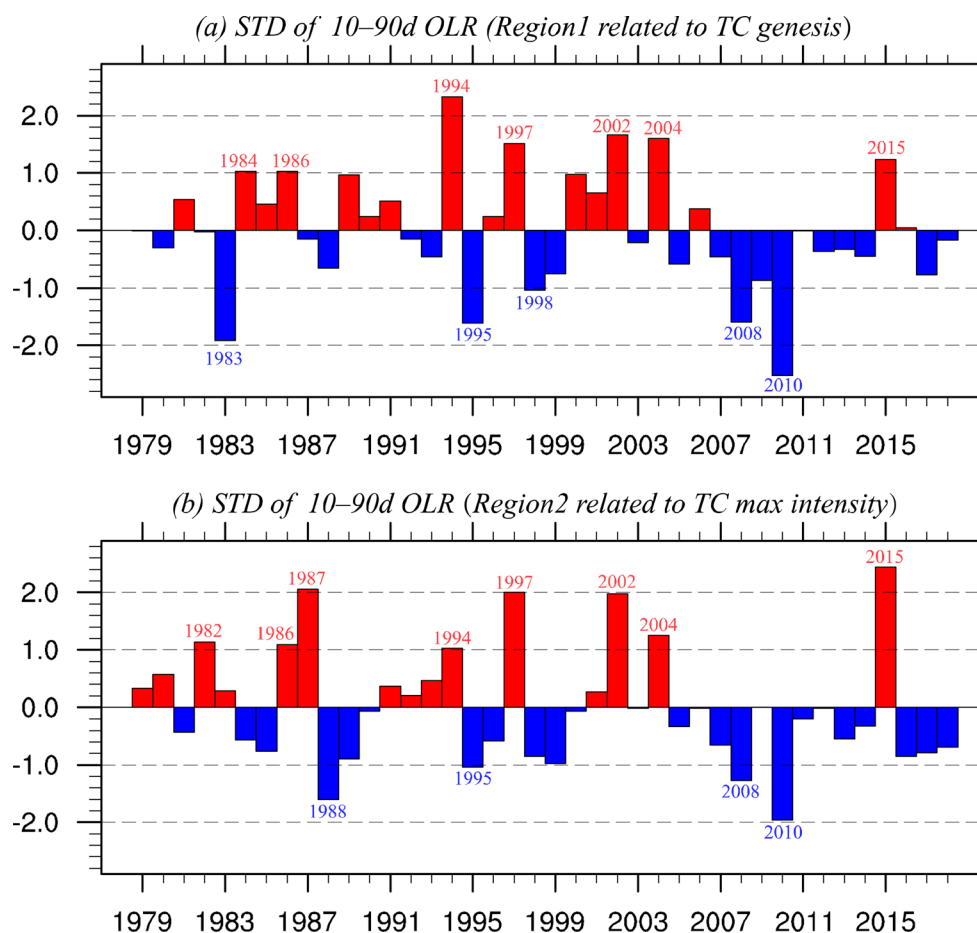genesis and TC maximum intensity, respectively. Blue characters mark the years with weakened BSISO (smaller than a standard deviation of normalized area-averaged BSISO amplitude) over the key region

(a) STD of 10–90d OLR (Region1 related to TC genesis)

(b) STD of 10–90d OLR (Region2 related to TC max intensity)

Table 1 (left) enhanced and weakened years of BSISO that are related to increased and decreased TC genesis counts, respectively. They are defined as when the BSISO amplitude is larger/smaller than $+1/-1$ standard deviation over the subtropical WNP (7.5°–27.5°N, 145°E–165°W), as shown in Fig. 3a. (right) as in the left column but for the enhanced and weakened BSISO years associated with inter-annual changes in TC maximum intensity (5°S–5°N, 140°E–160°W) displayed in Fig. 3b

	Associated with TC genesis count	Associated with TC max intensity
Enhanced BSISO years	1984, 1986, 1994, 1997, 2002, 2004, 2015	1982, 1986, 1987, 1994, 1997, 2002, 2004, 2015
Weakened BSISO years	1983, 1995, 1998, 2008, 2010	1988, 1995, 2008, 2010

4 Modulation of TC genesis by the BSISO at the interannual timescale

To understand how and through what physical processes the subtropical WNP BSISO exerts an impact on the basin-total TC genesis count at the interannual timescale, we compare the EKE budget terms (i.e., the energy sources for TC embryo development) during the enhanced and weakened BSISO years. To achieve this comparative analysis, we firstly categorized the summers with strong and weak BSISO amplitude over the key region of the subtropical

WNP (7.5°–27.5°N, 145°E–165°W; blue box in Fig. 2b). The enhanced and weakened BSISO years are defined by the normalized area-averaged BSISO amplitude (10–90-day OLR standard deviation for each summer) exceeding a standard deviation of $+1$ and -1, respectively (marked in red/blue font in Fig. 3a). The selected enhanced/weakened BSISO years are also listed in Table 1. Then, the distributions of EKE and WNP TC genesis during the enhanced and weakened BSISO years are compared in Fig. 4. Given that the <10-day high-pass filtered components include not only TCs but also convectively coupled equatorial waves, which may interact each other (Schreck et al. 2011; Wu and Takahashi 2018). To focus solely on the TC genesis–related changes, only the days when TCs form are used for the EKE composite. During years with enhanced BSISO over the subtropical WNP, the vigorous synoptic-scale disturbances related to TC embryos and TC genesis processes extend southeastward toward the eastern WNP (Fig. 4a). In contrast, the active EKE is confined to the western WNP during the weakened subtropical BSISO years (Fig. 4b). These patterns are highly consistent with the interannual changes in the distribution of TC genesis. More TCs form over the eastern tropical–subtropical WNP during the enhanced BSISO years (Fig. 4d) than the weakened BSISO years (Fig. 4e).
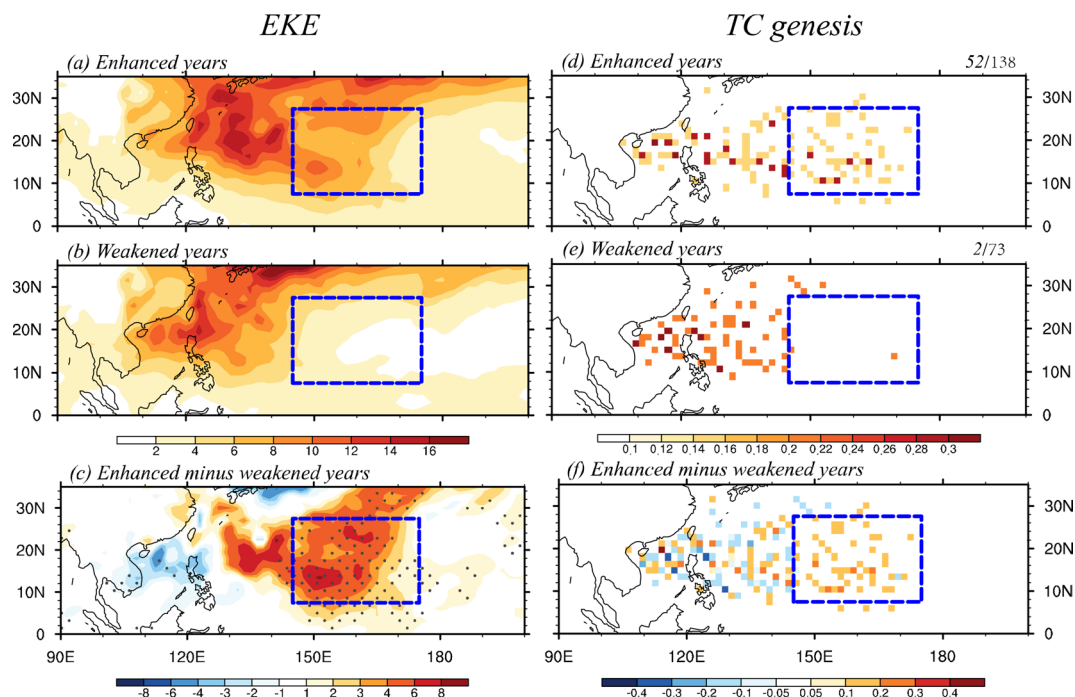
Fig. 4 Synoptic-scale EKE (shading; units: m² s⁻²) during the (**a**) enhanced and (**b**) weakened BSISO years identified in Fig. 3(a), and (**c**) their difference (enhanced years minus weakened years). To focus on the EKE pattern associated with TC genesis, only the EKE on days when a TC is generated was composited. Stippling in (**c**) denotes the differences between (**a**) and (**b**) are statistically significant at the 95% significance level. (**d–f**) Similar to (**a–c**) but for TC genesis frequency (shading; units: numbers). Blue boxes denote the regions with significant changes in EKE and TC genesis, which is the domain for the EKE budget analysis in Sect. 4. The ratios in the upper right corner of (**d**) and (**e**) represent the TC counts in the key region (blue boxes) versus the basin-total counts

Quantitatively, 52 and 2 TCs were observed over the eastern WNP (7.5°–27.5°N, 145°–175°E; outlined by the blue box), representing approximately 38% and 3% of TCs generated there, respectively, during the enhanced and weakened BSISO years. The results indicate that the synoptic-scale eddies associated with TC embryos over the key region (blue boxes in Fig. 4c, f) could be sufficiently energetic for growing into TCs when the BSISO is enhanced there (i.e., enhanced BSISO years), consistent with the results of Fig. 2b.

To identify the key processes contributing to the increased (decreased) TC genesis during the enhanced (weakened) BSISO years, the EKE budget equation is diagnosed over the regions with the significant EKE and TC changes (blue box in Fig. 4c and f). Note that only the days when TCs were generated are selected for energetic analysis (Fig. 5), in agreement with the composite approach of Fig. 4a and b. Because EKE shows a larger value and is closely linked with TC activities in the lower troposphere (Hsu et al. 2011), we focus on analyzing the 850-hPa EKE. By doing so, the eddy energetic processes are largely related to TC genesis. As expected, the synoptic-scale disturbances (TC embryos) could be sufficiently vigorous to develop into TCs over the eastern WNP when they have a higher growth rate of EKE ($\partial K'/\partial t$) during the years with enhanced BSISO

there (leftmost three bars in Fig. 5a). The enhanced EKE tendency during the enhanced BSISO years come not only from scale interaction processes, such as increased barotropic conversions from the background mean state and BSISO to eddies (CK_{M-E} and CK_{I-E}), but also the effect of eddy self-augmentation via the baroclinic energy conversion between EAPE and EKE (CE) and eddy geopotential flux (BG). CE is expected to be enhanced during TC genesis when the synoptic eddy embryos exhibit ascending motion accompanied by diabatic warming effects. Meanwhile, the convergence of low-pressure perturbations also contributes to enhancing the EKE through BG.

To understand how the seasonal-mean and BSISO flows influence the amplitude of EKE, we look closely at the individual terms of CK_{M-E} (Fig. 5b) and CK_{I-E} (Fig. 5c) during the enhanced/weakened BSISO years. The spatial distributions of the relevant terms are illustrated in Fig. 6. For CK_{M-E}, the eddy momentum fluxes acting on the zonal gradient of background mean zonal wind ($-u'u'\frac{\partial \bar{u}}{\partial x}$, the leftmost three bars in Fig. 5b) and on the meridional gradient of background mean zonal wind ($-u'v'\frac{\partial \bar{u}}{\partial y}$, the three bars of second term in Fig. 5b) can help synoptic eddies to obtain increased kinetic energy from the mean state. Although CK_{M-E} relies only on the processes of eddy momentum fluxes working with background mean flows [Eq. (2)], its
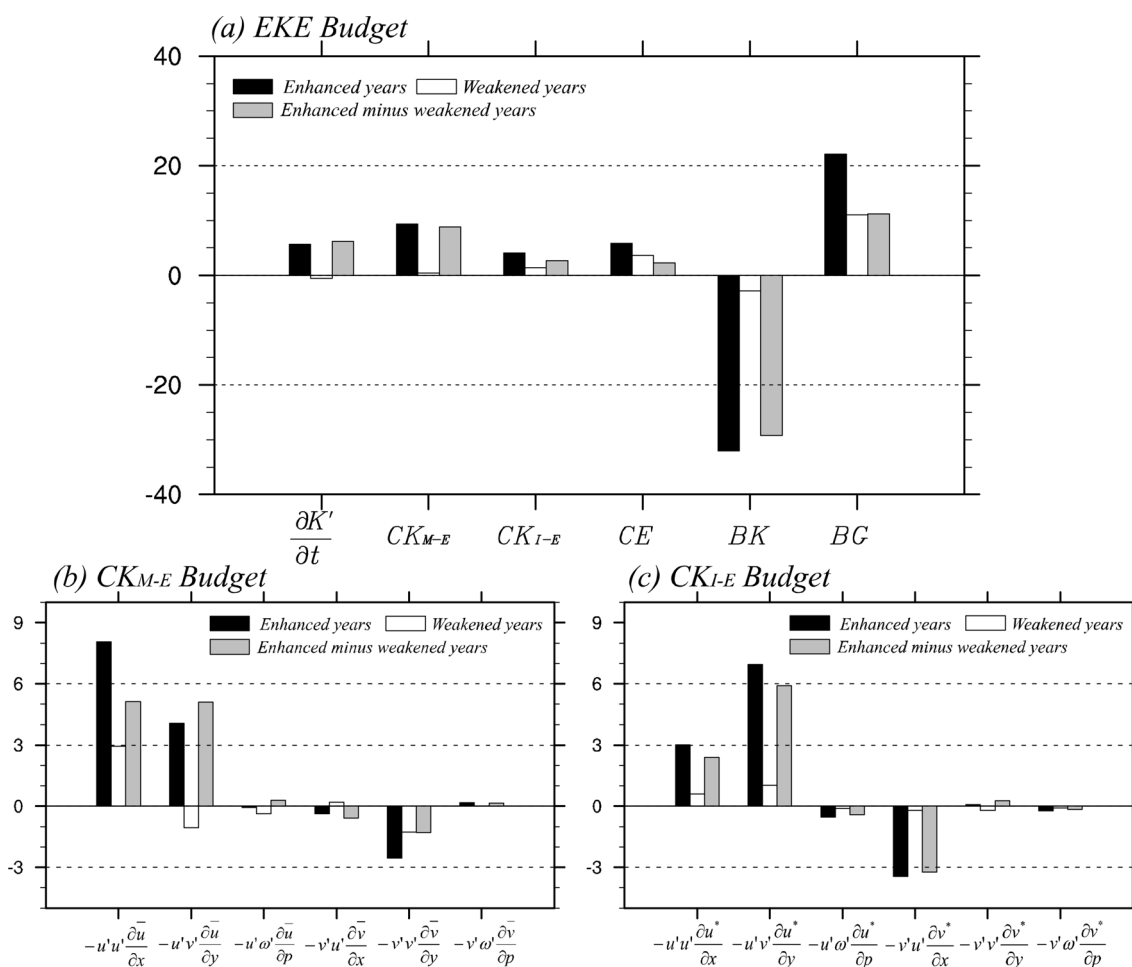
Fig. 5 (**a**) Averaged 850-hPa EKE tendency and budget terms over the eastern WNP (7.5°–27.5°N, 145°–175°E; blue boxes in Fig. 4) for days when TCs formed during enhanced (black bars) and weakened (white bars) BSISO years. Their differences are displayed by gray bars. From left to right: EKE tendency; barotropic energy conversion between mean flow and eddy; barotropic energy conversion between ISO and eddy; baroclinic energy conversion from EAPE to EKE; advection of EKE; and eddy geopotential flux. Units: 10^{-6} m^2 s^{-3}. (**b**) Individual terms of 850-hPa CK_{M-E} averaged over the region composited for BSISO active (black), inactive (white) years, and their difference (gray), respectively. (**c**) As in (**b**) but for the six leading individual terms of $CK_{I-E.}$

changes during the enhanced and weakened BSISO years implicitly suggest a complex scale interaction among the mean state, BSISO, and eddies over the WNP. The background mean states associated with the monsoon trough (marked by blue lines) and eddy activities varied with different interannual BSISO states. During the enhanced BSISO years, the region with enhanced eddy momentum ($u'u'$) extends southeastward (shading in Fig. 6a), where the convergent flows related to the eastward-extending monsoon trough strengthen (blue line in Fig. 6a). The interaction between zonal eddy momentum flux and zonal gradient of background zonal flow ($-u'u'\frac{\partial \bar{u}}{\partial x}$) produces a positive barotropic energy conversion, favoring the growth of eddies during enhanced BSISO years. Similarly, the meridional flux of zonal eddy momentum ($u'v'$) also tends to strengthen in the key region for enhanced BSISO years. Consequently, the cyclonic circulations of monsoon trough acting on the zonal

eddy momentum ($-u'v'\frac{\partial \bar{u}}{\partial y}$) contribute to maintain the EKE for enhanced BSISO years. In conclusion, compared to the weakened and restrict eddy momentum flux and westward-retreating monsoon trough during weakened BSISO years, the eddies are more effective in transferring the kinetic energy from the background flows during enhanced BSISO years. The importance of the monsoon trough on TC genesis has been widely documented in previous studies (Chen and Huang 2008; Wu et al. 2012), although changes in BSISO conditions were not considered.

Regarding the CK_{I-E}, only the six leading terms associated with eddy momentum flux acting on the BSISO anomalous flows (Tsou et al. 2014) are shown for comparison (Fig. 5c). The enhanced BSISO also directly contributes to the increased CK_{I-E} via increased barotropic energy conversion processes of $-u'u'\frac{\partial u^*}{\partial x}$ and $-u'v'\frac{\partial u^*}{\partial y}$ (Fig. 5c). The distributions of BSISO-related flows and eddy momentum

u'u' & >90d wind
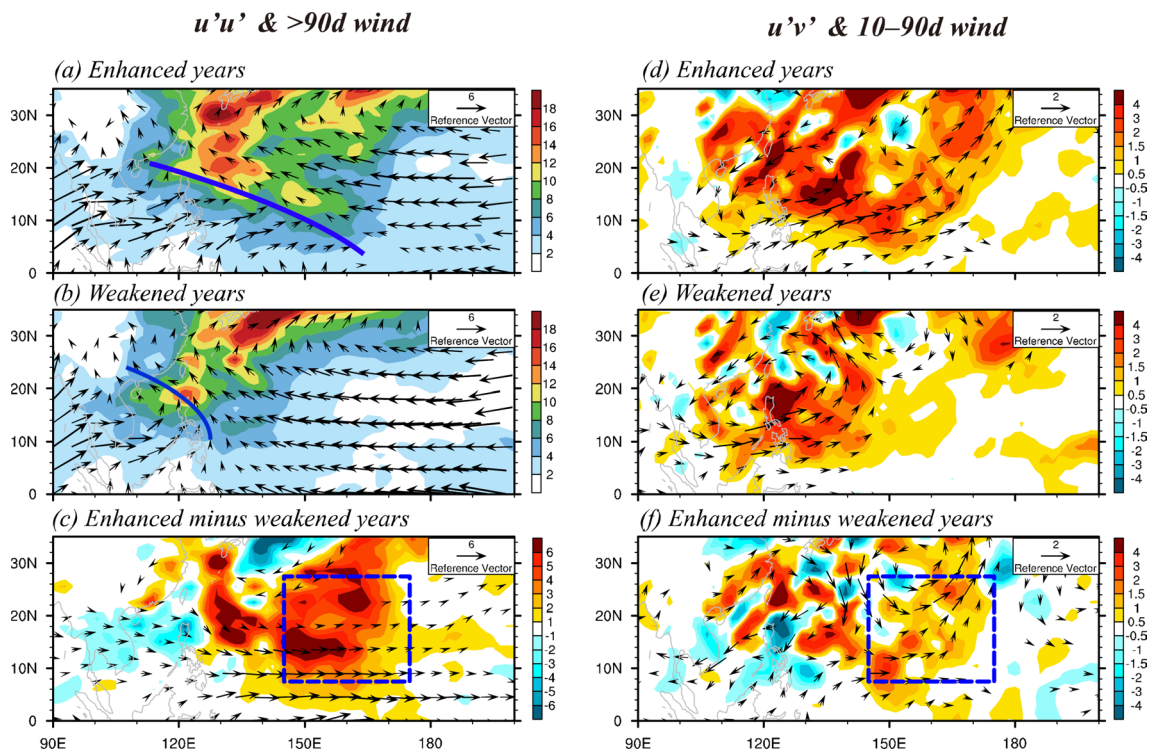
(a) Enhanced years

(b) Weakened years

(c) Enhanced minus weakened years

u'v' & 10–90d wind

(d) Enhanced years

(e) Weakened years

(f) Enhanced minus weakened years

Fig. 6 Zonal eddy momentum flux ($u'u'$) (shading; units: m² s⁻²) and background mean flows (vectors; units: m s⁻¹) for days when TCs formed during the (**a**) enhanced and (**b**) weakened BSISO years, and (**c**) their difference. (**d**–**f**) Similar to (**a**–**c**) but the shading represents the eddy momentum flux of $u'v'$ and the vectors denote the intraseasonal winds. The locations of monsoon trough during enhanced and weakened BSISO years are delineated by blue lines in (**a**) and (**b**), respectively

fluxes further elucidate how their interactions lead to the differences in barotropical conversion (Fig. 6). Benefited by the cyclonic circulation anomalies, the amplitude of eddy momentum fluxes ($u'u'$ and $u'v'$) over the key region is stronger (shading in Fig. 6) during the enhanced BSISO years than the weakened BSISO years. The interactions between convergent and cyclonic BSISO anomalies ($-\frac{\partial u^*}{\partial x} > 0$ and $-\frac{\partial u^*}{\partial y} > 0$) and enhanced eddy momentum fluxes generate an enhanced barotropic energy conversion for eddy growth. Given that the BSISO cyclonic anomaly is located over the northern WNP, the effect of zonal wind shear anomaly ($-u'u'\frac{\partial u^*}{\partial x}$) is slightly smaller than that of meridional wind shear anomaly ($-u'v'\frac{\partial u^*}{\partial y}$) over the key region for TC genesis (Fig. 5c).

In summary, the combined effects of the enhanced monsoon trough and cyclonic BSISO flow anomaly during the enhanced BSISO years help the TC embryos to develop efficiently into TCs over the eastern WNP, resulting in an overall increase in the TC genesis count over the WNP basin (blue boxes in Figs. 4 and 6).

The EKE diagnostic analyses (Figs. 4, 5 and 6) explain the interannual differences in the TC genesis count from the standpoint of eddy energetics, in particular the dynamic processes related to eddy momentum flux interacting with background flow anomalies. To discuss the contributions

of additional factors, such as the thermodynamic effect, to the BSISO–TC connection at the interannual timescale, we quantified the individual terms of the BSISO-related *GPI** [Eq. (6)]. Considering that GPI diagnosis emphasizes the large-scale effect, each term is composited over the TC formation region (including the grid cell with the TC center and the surrounding 3×3 grid). To reduce the uncertainty caused by the size of the diagnostic area, additional computations using a 5×5 and 7×7 grid were also performed (Fig. 7). The changes in *GPI** and individual terms for the two distinct BSISO conditions (enhanced minus weakened BSISO years) are compared. The resultant increased *GPI** (leftmost term in Fig. 7) confirms that the increased TC genesis count during the enhanced BSISO years is attributable to the anomalous environmental conditions related to the BSISO, regardless of the size of the diagnostic area. The complex nonlinear interactions among the various BSISO fields (rightmost term in Fig. 7) are the most important contributors. As for the BSISO impact via a single field (the middle five terms), the enhanced vorticity, humidity and vertical motion related to strengthened BSISO over the subtropical WNP all show positive contributions. This result also supports the finding of the EKE diagnosis, i.e., that the cyclonic and convergent (possibly linked with the vertical motion anomaly) flows play a crucial role in the increased

Fig. 7 Relative contributions of individual terms to the differences in *GPI** when TCs generated during the enhanced BSISO years relative to weakened BSISO years (enhanced minus weakened years), defined in Fig. 3a. Black, white, and gray bars denote the results based on the area averages of variables using a 3×3, 5×5, and 7×7 grid box from the TC center. From left to right: total changes in *GPI**; contributions from the changes in BSISO-related vorticity; relative humidity; potential intensity; vertical wind shear; vertical motion; and nonlinear processes
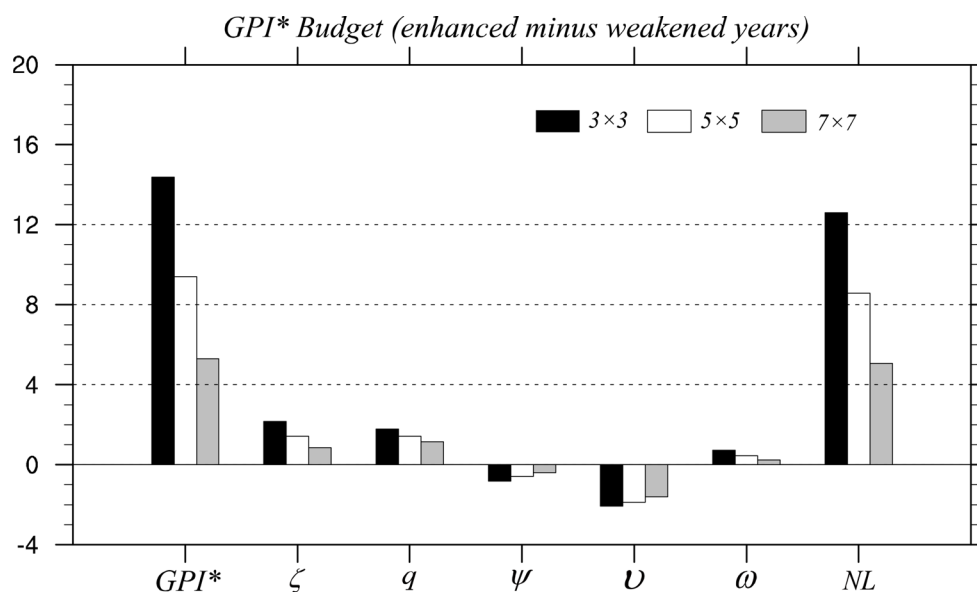
TC genesis count during the enhanced BSISO years. The circulation anomalies also favor increases in moisture convergence and lower-to-mid tropospheric moistening for TC genesis as well (Wang et al. 2018; Wang and Murakami 2020). Notably, the MPI contribution exhibits negative values, suggesting that SST and the temperature profile may not be the primary factors influencing TC genesis. The results of Fig. 7 remain consistent when we repeated the analysis of *GPI** using the data with TC removals.

In summary, the interannual changes in WNP TC genesis count are not solely determined by the seasonal anomalies (Chia and Ropelewski 2002; Chen et al. 2006; Camargo et al. 2007; Wang et al. 2013), but also by the BSISO amplitude over the subtropical WNP. The enhanced BSISO creates a favorable environment for TC embryos to grow into a TC through local dynamic and thermodynamic effects (Figs. 4, 5, 6 and 7). Although the results are consistent with previous observational and modeling results that disentangled the climatological effect of the BSISO on TC genesis (Tsuboi and Takemi 2014; Cao et al. 2014, 2021), here we further highlight the BSISO–TC linkage at the interannual timescale, involving a more complicated interaction among the background mean flow, BSISO and eddies.

5 Modulation of TC intensification by the BSISO at the interannual timescale

Different from the interannual impact of the subtropical WNP BSISO on the TC genesis count (Fig. 2b), the year-to-year changes in TC maximum intensity are related to the central-western equatorial BSISO amplitude (Fig. 2c). As discussed earlier in Sect. 3, the higher intensity of WNP TCs could be linked with the contribution of their longer

lifespans (Fig. 2d). This suggestion is again supported by the composites of TC track and intensity during the years with enhanced and weakened BSISO over the central-western equatorial Pacific (Fig. 8a, b), according to the classification results in Fig. 3b; Table 1. During the enhanced BSISO years related to maximum TC intensity, most TCs form over the southeastern WNP where the BSISO is active (Fig. 8a). A large portion of TCs reach their maximum intensity as intense typhoons (C4–C5, red dots in Fig. 8a) as they stay longer over the open ocean (average lifespan is 6.88 days). In contrast, the weakened BSISO over the central-western equatorial Pacific reduces TC genesis there (Fig. 8b). The shorter duration of TCs (average lifespan is 4.68 days) inhibits the probability of intense typhoon occurrence (fewer red dots in Fig. 8b).

The central-western equatorial BSISO benefits not only the TC generation there but also the enhancement of TC intensification (Fig. 8a, b). To elucidate the processes accounting for TC intensification, we apply EKE analysis along the TC track during the stages of intensification. By doing this, the processes of eddy energetics along the TC track can be used to explain the sources of energy for TC intensification. The distributions of EKE are consistent with the behaviors of TCs, with increased amplitude over the entire basin when the BSISO is enhanced over the central-western equatorial Pacific (Fig. 8c, d). These TCs have a larger intensification rate ($\partial K'/\partial t$) before their intensity reaches the maximum (leftmost bar in Fig. 9a). Both the increased barotropic conversion (terms CK_{M-E} and CK_{I-E}) and eddy–eddy processes related to EAPE-to-EKE conversion (term CE) reveal positive contributions to a higher intensification rate of eddies during the enhanced BSISO years. These three processes are commonly recognized as the major sources of eddy intensification. Baroclinic energy
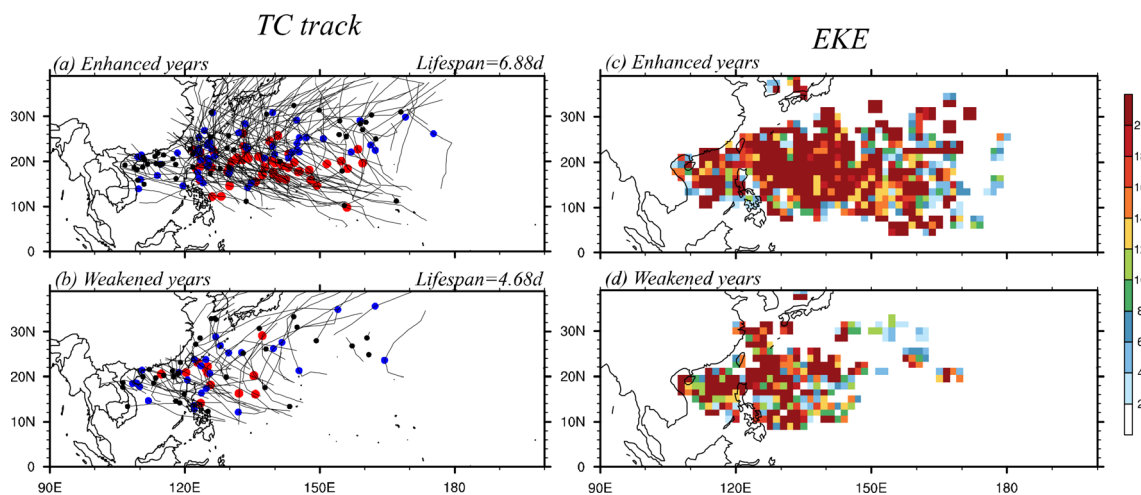
Fig. 8 TC tracks and intensities during the (**a**) enhanced and (**b**) weakened BSISO years related to interannual changes in TC maximum intensity, categorized by the results of Fig. 3b. The locations of the maximum intensity occurrence are denoted by colored dots (black dots, TS; blue dots, C1–C3; red dots, C4–C5). The average TC lifespan is shown in the top-right corner of each panel. EKE (shading; units: $m^2\ s^{-2}$) along the TC tracks during the stages of intensification during (**c**) enhanced and (**d**) weakened BSISO years related to interannual changes in TC maximum intensity
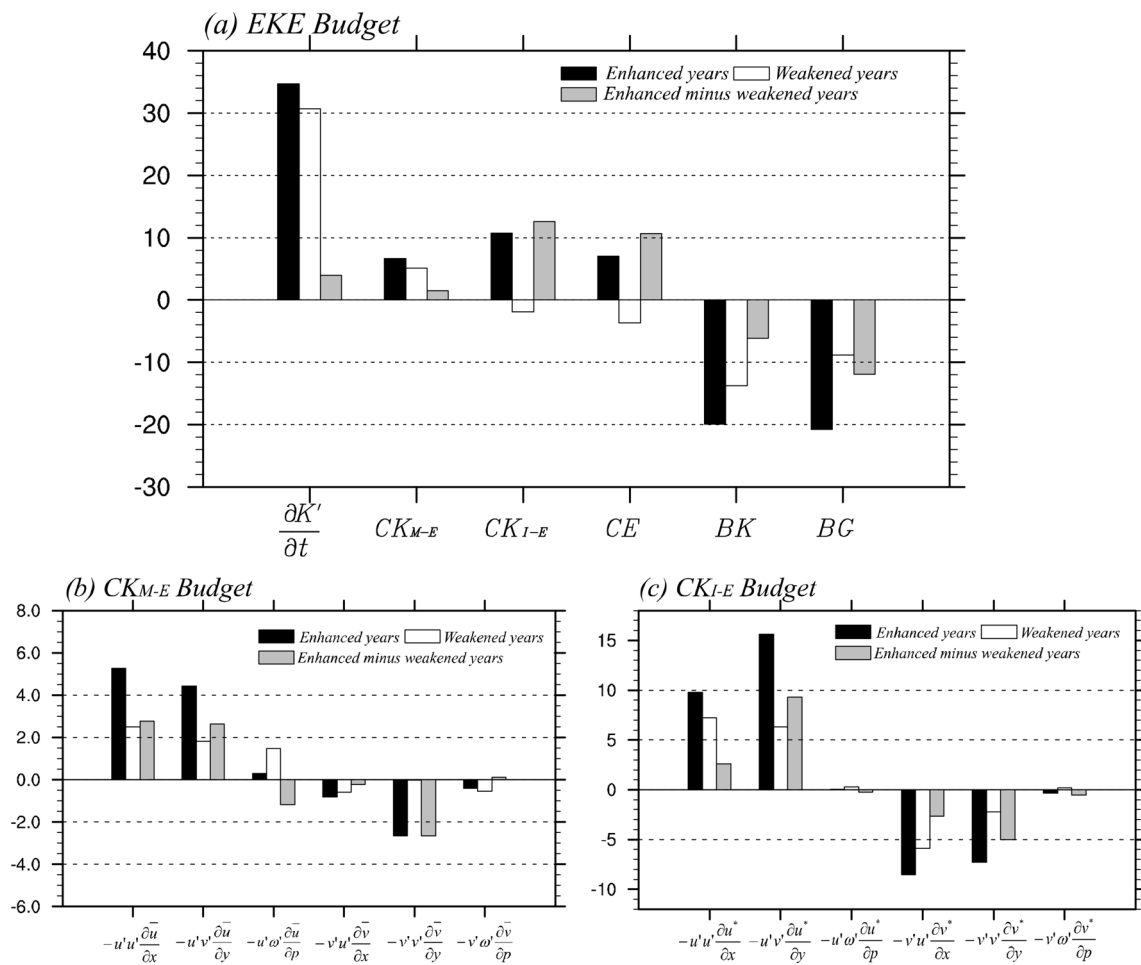
Fig. 9 (**a**) 850-hPa EKE tendency and its budget terms averaged along the TC tracks for TC intensifying days during BSISO active (black), inactive (white) years related to TC maximum intensity, and their difference (gray). Units: $10^{-5}\ m^2\ s^{-3}$. (**b**) Individual terms of 850-hPa CK_{M-E} composited for BSISO active (black), inactive (white) years, and their difference (gray), respectively. (**c**) As in (**b**) but for the six leading individual terms of CK_{I-E}.

conversion (CE) occurs during the TC intensification stage as TCs experience upward motion concurrent with diabatic heating associated with condensation. With a focus on the barotropic energy conversion related to scale interaction, the individual terms of CK_{M-E} and CK_{I-E} are compared (Fig. 9b, c). Regarding the enhanced background mean flow-to-EKE conversion (term CK_{M-E}), the eddy momentum fluxes working on zonal and meridional gradients of >90-day background zonal wind ($-u'u'\frac{\partial \bar{u}}{\partial x}$ and $-u'v'\frac{\partial \bar{u}}{\partial y}$) are the leading contributors (Fig. 9b). Similarly, the eddies interacting with the zonal and meridional gradients of BSISO zonal wind perturbations ($-u'u'\frac{\partial u^*}{\partial x}$ and $-u'v'\frac{\partial u^*}{\partial y}$) also dominate the increased CK_{I-E} during the enhanced BSISO years (Fig. 9c).

Figures 10 and 11 display the distributions of eddy, BSISO, and background flow components associated with barotropic energy conversions during the BSISO years favorable and unfavorable for TC intensification. Accompanied by enhanced BSISO over the central-western equatorial Pacific, eddy momentum fluxes ($u'u'$ and $u'v'$) show stronger amplitude and extend southeastward toward the central-western equatorial Pacific (Fig. 10). Since the flow patterns become less-organized based on the spatial composite analysis, we therefore analyze the probability distribution functions of 850-hPa divergence and vorticity associated with the seasonal background flow and BSISO perturbations (i.e., effects of $\frac{\partial \bar{u}}{\partial x}$, $\frac{\partial \bar{u}}{\partial y}$, $\frac{\partial u^*}{\partial x}$, and $\frac{\partial u^*}{\partial y}$) to understand their contributions to the enhanced barotropic energy conversion process. During the intensification stage, the eddies (TCs) have higher probabilities to be embedded in the enhanced convergent ($-\frac{\partial \bar{u}}{\partial x}>0$) and cyclonic ($-\frac{\partial \bar{u}}{\partial y}>0$) circulations during the enhanced BSISO years (red curves in Fig. 11a and c). Meanwhile, vigorous BSISO-related convergent ($-\frac{\partial u^*}{\partial x}>0$) and cyclonic ($-\frac{\partial u^*}{\partial y}>0$) anomalies are

also more frequent along the TC track during the enhanced BSISO years (red curves in Fig. 11b and d). These circulation conditions are conducive to the eddies intensifying and reaching a larger TC amplitude (Fig. 8a, b). In addition to atmospheric processes, we examined the effects of BSISO-related oceanic anomalies on TC intensification at the interannual timescale. The results indicate that oceanic conditions, including MPI and TC heat potential anomalies associated with the BSISO, contribute insignificantly and negatively to TC intensification at the interannual timescale (not shown). Note that the results remain consistent even if we include the additional step of removing TCs before time-filtering and composite analysis, indicating the robustness of our conclusions.

6 Summary and discussion

The WNP is a unique basin with the most vigorous TC and BSISO activities, which both experience interannual variability (Chia and Ropelewski 2002; Chen et al. 2006; Li and Zhou 2012; Wu and Cao 2017; Wang and Wu 2020; Kikuchi 2021; Cao et al. 2021). Previous studies have discussed at length, but separately, the interannual changes in TC activity (Chia and Ropelewski 2002; Chen et al. 2006; Li and Zhou 2012) and BSISO (Wu and Cao 2017; Wang and Wu 2020; Kikuchi 2021), as well as the effects of ENSO states (Wang and Chan 2002; Chia and Ropelewski 2002; Camargo et al. 2007; Li and Zhou 2012). Considering that a close connection between TCs and BSISO was found (Maloney and Hartmann 2001; Hall et al. 2001; Hsu et al. 2011; Li and Zhou 2013; Zhao et al. 2015; Kikuchi 2021), whether and how the year-to-year variations of BSISO (whose regional changes may not be completely controlled by ENSO; Cao
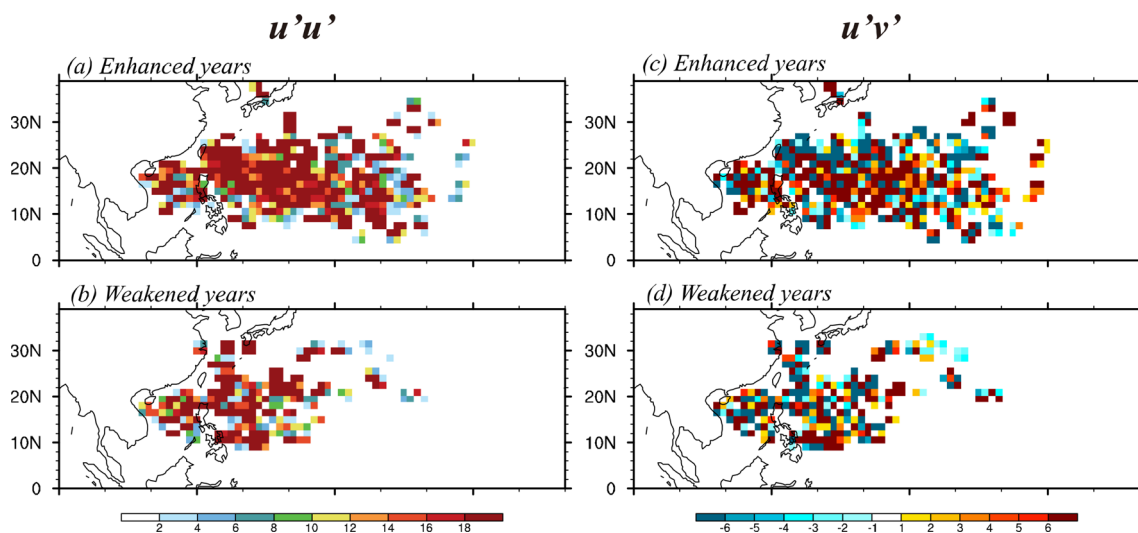

Fig. 10 Zonal eddy momentum flux ($u'u'$) (shading; units: $m^2\,s^{-2}$) composited along the TC tracks when TCs intensified during the (**a**) enhanced and (**b**) weakened BSISO years. (**c, d**) Similar to (**a, b**) but the shading represents the eddy momentum flux of $u'v'$

Fig. 11 Probability density function of the (**a**) seasonal background mean (> 90-day) and (**b**) 10–90-day divergence (units: s^{-1}). (**c, d**) Similar to (**a, b**) but for the (**c**) seasonal background mean and (**d**) 10–90-day vorticity (units: s^{-1})
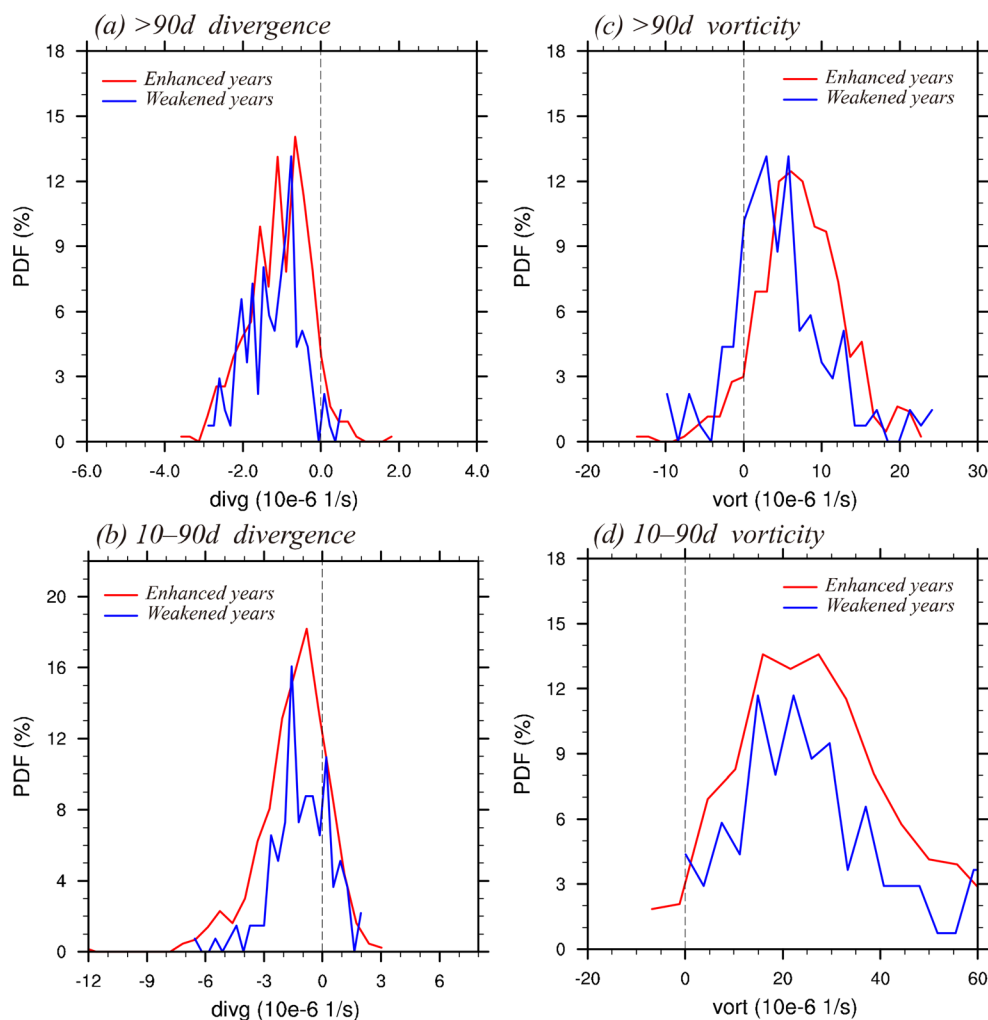
et al. 2021) exert influences on interannual changes in TC genesis counts and intensity over the WNP, is still an open question. Based on statistical analysis and eddy energetic diagnosis, the BSISO–TC connection at the interannual timescale was investigated in this study. The main findings can be summarized as follows.

Based on correlation analysis of the year-to-year variations in BSISO amplitude and TC activities, we found that the interannual changes in TC genesis counts and intensity are modulated by the BSISO over different regions of the WNP (Fig. 2). The May–October BSISO amplitude over the subtropical WNP (7.5°–27.5°N, 145°E–165°W) is positively correlated with the TC genesis count over the eastern WNP, where abnormally increased (very few) TC generations are apparent during years with enhanced (weakened) BSISO over the subtropical WNP (Figs. 2b and 4). Consequently, an increase in the basin-total TC count is observed during years with enhanced BSISO over the subtropical WNP. In contrast, the maximum intensity that TCs can reach is influenced by the BSISO amplitude over the central-western equatorial Pacific (5°S–5°N, 140°E–160°W)

during May–October (Fig. 2c). In summers with enhanced BSISO over the central-western equatorial Pacific, TCs tend to form more frequently over the southeastern WNP and intensify quickly (Fig. 8). These TCs have a higher chance of reaching the intensity level of intense typhoons. When we consider only the years with significant BSISO signals but with neutral ENSO conditions, the behaviors of TC activity exhibit similar changes (not shown). The sensitivity tests for defining the BSISO components, whether including or excluding daily variability related to ENSO (i.e., daily fields regressed on the Niño-3.4 index), also yield consistent results. These indicate that the interannual BSISO–TC connection remains robust, even without the contribution of ENSO.

The modulation of TC genesis counts by BSISO at the interannual timescale was diagnosed by the EKE budget (Figs. 5 and 6) and intraseasonal GPI variability (Fig. 7) based on the days with TC genesis. From the viewpoint of eddy energetics, TC embryos (synoptic-scale eddies) can gain more kinetic energy to grow into TCs from both the background mean flow and the BSISO circulation anomalies

(CK_{M-E} and CK_{I-E}) over the subtropical WNP; they can also sustain their growth by self-augmentation processes (CE and BG) (Fig. 5). During summers with enhanced BSISO, the eastward extension of both the monsoon trough and vigorous BSISO region contributes to the enhanced CK_{M-E} and CK_{I-E} by working on the strengthened eddy momentum. This suggests a complex interaction among mean flow, BSISO, and eddies. Besides the contribution of circulation anomalies (i.e., the dynamic effect), enhanced BSISO also favors TC genesis via providing increased humidity in the lower and middle troposphere during enhanced BSISO years, as displayed by the analysis results of GPI^* (Fig. 7). To elucidate the TC intensification mechanism related to interannual BSISO changes, we conducted EKE diagnosis for understanding the energy sources along the TC tracks. When the central-western equatorial BSISO is enhanced, TCs tend to form in the southeastern WNP and persist for longer over the ocean before reaching a maximum intensity (Fig. 8). Rather than focusing on local effects, the equatorial BSISO controls large-scale background states, which in turn affects TC activity. During the TC intensification stage, these eddies also obtain more energy to intensify through the increased barotropic energy conversion (Fig. 9), as higher amplitudes and probabilities of cyclonic and convergent flows related to the background seasonal and BSISO flows appear during enhanced BSISO years compared with weakened BSISO years (Figs. 10 and 11).

Although these BSISO-related processes affecting the TC genesis and intensification rates at the interannual timescale are generally consistent with climatological studies that have discussed the BSISO–TC relationship over the whole basin (Maloney and Hartmann 2001; Hsu et al. 2011; Li and Zhou 2013; Kikuchi 2021), our study further unveils the effects of regional BSISO on TC activities at the interannual timescale. This raises an open issue regarding the mechanisms responsible for the interannual changes in vigorous BSISO locations (subtropical WNP vs. central-western equatorial Pacific) that exert different influences on TC genesis counts and intensity. Our recent study, Zhou et al. (2024), has addressed this emergent issue. We found that the amplitude of the subtropical BSISO, which influences interannual changes in WNP TC genesis counts, is linked both to the interannual variations of equatorial central-eastern Pacific SST associated with ENSO and to subtropical eastern Pacific SST, known as the PMM (Chiang and Vimont 2004). In contrast, results from partial correlation analysis indicate that the interannual variations in equatorial BSISO amplitude are more closely related to the ENSO signal (Teng and Wang 2003; Li and Mao 2019) rather than the PMM. These findings, along with the results presented in this study, suggest complex scale interactions over the WNP. The interannual SST modes exert both remote and local influences on BSISO and TC activities, as well as on the BSISO–TC linkage.

Differing from the previous studies that mainly focus on interactions between two components (such as ENSO–TC and ENSO–BSISO connections), the broader perspective on scale interaction among interannual SST modes, BSISO, and TC activities over the WNP summer monsoon region advances our understanding of the mechanisms driving interannual TC variations by considering the effect of interannual BSISO variability. This consideration also provides guidance for improving the prediction accuracy of WNP TC activities, assuming that numerical models can better capture the multi-scale interaction processes. Investigating how the prediction skill of the ENSO/PMM–BSISO interaction influences the accuracy of TC forecasts is a worthwhile direction for further investigation.

Declarations

Ethical approval Not applicable to this article.

Conflict of interest The authors declare that they have no conflicts of interest.

References

Bell GD, Halpert MS, Schnell RC et al (2000) Climate assessment for 1999. Bull Am Meteorol Soc 81:S1–S50. https://doi.org/10.1175/1520-0477(2000)81[s1:CAF]2.0.CO;2

Bister M, Emanuel KA (1998) Dissipative heating and hurricane intensity. Meteorol Atmos Phys 65:233–240. https://doi.org/10.1007/BF01030791

Camargo SJ, Polvani LM (2019) Little evidence of reduced global tropical cyclone activity following recent volcanic eruptions. Npj Clim Atmos Sci 2:14. https://doi.org/10.1038/s41612-019-0070-z

Camargo SJ, Emanuel KA, Sobel AH (2007) Use of a genesis potential index to diagnose ENSO effects on tropical cyclone genesis. J Clim 20:4819–4834. https://doi.org/10.1175/JCLI4282.1

Cao X, Li T, Peng M et al (2014) Effects of monsoon trough intraseasonal oscillation on tropical cyclogenesis over the western North Pacific. J Atmos Sci 71:4639–4660. https://doi.org/10.1175/JAS-D-13-0407.1

Cao X, Wu R, Wei N, Dai Y (2020) Location of the preferred region for tropical cyclogenesis in strong monsoon trough pattern over the western North Pacific. J Meteorol Soc Jpn Ser II 98:637–654. https://doi.org/10.2151/jmsj.2020-034

Cao X, Wu R, Xu J et al (2021) Contribution of the intensity of intraseasonal oscillation to the interannual variation of tropical cyclogenesis over the western North Pacific. Environ Res Commun 3:031002. https://doi.org/10.1088/2515-7620/abed93

Chan JCL (1985) Tropical cyclone activity in the Northwest Pacific in relation to the El Niño/Southern Oscillation phenomenon. Mon Weather Rev 113:599–606. https://doi.org/10.1175/1520-0493(1985)113%3C0599:TCAITN%3E2.0.CO;2

Chen G, Huang R (2008) Influence of monsoon over the warm pool on interannual variation on tropical cyclone activity over the western North Pacific. Adv Atmos Sci 25:319–328. https://doi.org/10.1007/s00376-008-0319-7

Chen G, Huang R (2009) Interannual variations in mixed Rossby–gravity waves and their impacts on tropical cyclogenesis over the western North Pacific. J Clim 22:535–549. https://doi.org/10.1175/2008JCLI2221.1

Chen T-C, Wang S-Y, Yen M-C (2006) Interannual variation of the tropical cyclone activity over the western North Pacific. J Clim 19:5709–5720. https://doi.org/10.1175/JCLI3934.1

Chen X, Li C, Tan Y (2015) The influence of El Niño on MJO over the equatorial Pacific. J Ocean U China 14:1–8. https://doi.org/10.1007/s11802-015-2381-y

Chen X, Li C, Li X (2020) Influences of ENSO on boreal summer intraseasonal oscillation over the western Pacific in decaying summer. Clim Dyn 54:3461–3473. https://doi.org/10.1007/s00382-020-05183-9

Chia HH, Ropelewski CF (2002) The interannual variability in the genesis location of tropical cyclones in the Northwest Pacific. J Clim 15:2934–2944. https://doi.org/10.1175/1520-0442(2002)015%3C2934:TIVITG%3E2.0.CO;2

Chiang JCH, Vimont DJ (2004) Analogous Pacific and atlantic meridional modes of tropical atmosphere–ocean variability*. J Clim 17:4143–4158. https://doi.org/10.1175/JCLI4953.1

Dee DP, Uppala SM, Simmons AJ et al (2011) The ERA-Interim reanalysis: configuration and performance of the data assimilation system. Q J Roy Meteor Soc 137:553–597. https://doi.org/10.1002/qj.828

Duchon CE (1979) Lanczos filtering in one and two dimensions. J Appl Meteorol Clim 18:1016–1022. https://doi.org/10.1175/1520-0450(1979)018%3C1016:LFIOAT%3E2.0.CO;2

Emanuel K (1995) Sensitivity of tropical cyclones to surface exchange coefficients and a revised steady-state model incorporating eye dynamics. J Atmos Sci 52:3969–3976. https://doi.org/10.1175/1520-0469(1995)052%3C3969:SOTCTS%3E2.0.CO;2

Emanuel K, Nolan D (2004) Tropical cyclone activity and global climate. Bull Amer Meteorol Soc 85:240–241

Emanuel K, Zhang F (2017) The role of inner-core moisture in tropical cyclone predictability and practical forecast skill. J Atmos Sci 74:2315–2324. https://doi.org/10.1175/JAS-D-17-0008.1

Gao J, Li T (2011) Factors controlling multiple tropical cyclone events in the western North Pacific. Mon Weather Rev 139:885–894. https://doi.org/10.1175/2010MWR3340.1

Hall JD, Matthews AJ, Karoly DJ (2001) The modulation of tropical cyclone activity in the Australian region by the Madden–Julian oscillation. Mon Weather Rev 129:2970–2982. https://doi.org/10.1175/1520-0493(2001)129%3C2970:TMOTCA%3E2.0.CO;2

Hsu H-H, Hung C-H, Lo A-K et al (2008) Influence of tropical cyclones on the estimation of climate variability in the tropical western North Pacific. J Clim 21:2960–2975. https://doi.org/10.1175/2007JCLI1847.1

Hsu P-C, Tsou C-H, Hsu H-H, Chen J-H (2009) Eddy energy along the tropical storm track in association with ENSO. J Meteorol Soc Jpn Ser II 87:687–704. https://doi.org/10.2151/jmsj.87.687

Hsu P-C, Li T, Tsou C-H (2011) Interactions between boreal summer intraseasonal oscillations and synoptic-scale disturbances over the western North Pacific. Part I: energetics diagnosis*. J Clim 24:927–941. https://doi.org/10.1175/2010JCLI3833.1

Hsu P-C, Lee T-H, Tsou C-H et al (2017) Role of scale interactions in the abrupt change of tropical cyclone in autumn over the western North Pacific. Clim Dyn 49:3175–3192. https://doi.org/10.1007/s00382-016-3504-x

Jiang X, Zhao M, Waliser DE (2012) Modulation of tropical cyclones over the eastern Pacific by the intraseasonal variability simulated in an AGCM. J Clim 25:6524–6538. https://doi.org/10.1175/JCLI-D-11-00531.1

Kikuchi K (2021) The boreal summer intraseasonal oscillation (BSISO): a review. J Meteorol Soc Jpn Ser II 99:933–972. https://doi.org/10.2151/jmsj.2021-045

Kurihara Y, Bender MA, Tuleya RE, Ross RJ (1995) Improvements in the GFDL hurricane prediction system. Mon Weather Rev 123:2791–2801. https://doi.org/10.1175/1520-0493(1995)123%3C2791:IITGHP%3E2.0.CO;2

Li C (1988) Actions of typhoons over the western Pacific (including the South China Sea) and El Nino. Adv Atmos Sci 5:107–115. https://doi.org/10.1007/BF02657352

Li J, Mao J (2019) Factors controlling the interannual variation of 30–60-day boreal summer intraseasonal oscillation over the Asian summer monsoon region. Clim Dyn 52:1651–1672. https://doi.org/10.1007/s00382-018-4216-1

Li RCY, Zhou W (2012) Changes in western Pacific tropical cyclones associated with the El Niño–Southern Oscillation cycle. J Clim 25:5864–5878. https://doi.org/10.1175/JCLI-D-11-00430.1

Li RCY, Zhou W (2013) Modulation of western North Pacific tropical cyclone activity by the ISO. Part I: genesis and intensity. J Clim 26:2904–2918. https://doi.org/10.1175/JCLI-D-12-00210.1

Li RCY, Zhou W, Chan JCL, Huang P (2012) Asymmetric modulation of western North Pacific cyclogenesis by the Madden–Julian oscillation under ENSO conditions. J Clim 25:5374–5385. https://doi.org/10.1175/JCLI-D-11-00337.1

Liebmann B, Smith CA (1996) Description of a complete (interpolated) outgoing longwave radiation dataset. Bull Amer Meteorol Soc 77:1275–1277

Lin H (2019) Long-lead ENSO control of the boreal summer intraseasonal oscillation in the East Asian-western North Pacific region. Npj Clim Atmos Sci 2:31. https://doi.org/10.1038/s41612-019-0088-2

Lin A, Li T (2008) Energy spectrum characteristics of boreal summer intraseasonal oscillations: climatology and variations during the ENSO developing and decaying phases. J Clim 21:6304–6320. https://doi.org/10.1175/2008JCLI2331.1

Maloney ED, Hartmann DL (2001) The Madden–Julian oscillation, barotropic dynamics, and North Pacific tropical cyclone formation. Part I: observations. J Atmos Sci 58:2545–2558. https://doi.org/10.1175/1520-0469(2001)058%3C2545:TMJOBD%3E2.0.CO;2

Murakami H, Wang B (2010) Future change of North Atlantic tropical cyclone tracks: projection by a 20-km-mesh global atmospheric model. J Clim 23:2699–2721. https://doi.org/10.1175/2010JCLI3338.1

Murakami H, Li T, Hsu P-C (2014) Contributing factors to the recent high level of accumulated cyclone energy (ACE) and power dissipation index (PDI) in the North Atlantic. J Clim 27:3023–3034. https://doi.org/10.1175/JCLI-D-13-00394.1

Qian Y, Murakami H, Nakano M et al (2019) On the mechanisms of the active 2018 tropical cyclone season in the North Pacific. Geophys Res Lett 46:12293–12302. https://doi.org/10.1029/2019GL084566

Schreck CJ, Molinari J, Mohr KI (2011) Attributing tropical cyclogenesis to equatorial waves in the western North Pacific. J Atmos Sci 68:195–209. https://doi.org/10.1175/2010JAS3396.1

Sobel AH, Wing AA, Camargo SJ et al (2021) Tropical cyclone frequency. Earths Future 9. https://doi.org/10.1029/2021EF002275. e2021EF002275

Teng H, Wang B (2003) Interannual variations of the boreal summer intraseasonal oscillation in the Asian–Pacific region. J Clim 16:3572–3584. https://doi.org/10.1175/1520-0442(2003)016%3C3572:IVOTBS%3E2.0.CO;2

Trabing BC, Musgrave KD, DeMaria M et al (2023) The development and evaluation of a tropical cyclone probabilistic landfall forecast product. Weather Forecast 38:1363–1374. https://doi.org/10.1175/WAF-D-22-0199.1

Tsou C-H, Hsu H-H, Hsu P-C (2014) The role of multiscale interaction in synoptic-scale eddy kinetic energy over the western North Pacific in autumn. J Clim 27:3750–3766. https://doi.org/10.1175/JCLI-D-13-00380.1

Tsuboi A, Takemi T (2014) The interannual relationship between MJO activity and tropical cyclone genesis in the Indian Ocean. Geosci Lett 1:9. https://doi.org/10.1186/2196-4092-1-9

Wang B, Chan JCL (2002) How strong ENSO events affect tropical storm activity over the western North Pacific. J Clim 15:1643–1658. https://doi.org/10.1175/1520-0442(2002)015%3C1643:HSEEAT%3E2.0.CO;2

Wang B, Murakami H (2020) Dynamic genesis potential index for diagnosing present-day and future global tropical cyclone genesis. Environ Res Lett 15:114008. https://doi.org/10.1088/1748-9326/abbb01

Wang C, Wu L (2016) Interannual shift of the tropical upper-tropospheric trough and its influence on tropical cyclone formation over the western North Pacific. J Clim 29:4203–4211. https://doi.org/10.1175/JCLI-D-15-0653.1

Wang Y, Wu R (2020) Patterns and factors of interannual variations of boreal summer intraseasonal oscillation intensity over tropical western North Pacific. Clim Dyn 54:2085–2099. https://doi.org/10.1007/s00382-019-05100-9

Wang C, Li C, Mu M, Duan W (2013) Seasonal modulations of different impacts of two types of ENSO events on tropical cyclone activity in the western North Pacific. Clim Dyn 40:2887–2902. https://doi.org/10.1007/s00382-012-1434-9

Wang Q, Li J, Li Y et al (2018) Modulation of tropical cyclogenesis location and frequency over the Indo–western North Pacific by the intraseasonal Indo–western Pacific convection oscillation during the boreal extended summer. J Clim 31:1435–1450. https://doi.org/10.1175/JCLI-D-17-0085.1

Webster PJ, Holland GJ, Curry JA, Chang H-R (2005) Changes in tropical cyclone number, duration, and intensity in a warming environment. Science 309:1844–1846. https://doi.org/10.1126/science.1116448

Wu R, Cao X (2017) Relationship of boreal summer 10–20-day and 30–60-day intraseasonal oscillation intensity over the tropical western North Pacific to tropical Indo-Pacific SST. Clim Dyn 48:3529–3546. https://doi.org/10.1007/s00382-016-3282-5

Wu L, Takahashi M (2018) Contributions of tropical waves to tropical cyclone genesis over the western North Pacific. Clim Dyn 50:4635–4649. https://doi.org/10.1007/s00382-017-3895-3

Wu L, Wang B (2004) Assessing impacts of global warming on tropical cyclone tracks. J Clim 17:1686–1698. https://doi.org/10.1175/1520-0442(2004)017%3C1686:AIOGWO%3E2.0.CO;2

Wu L, Wen Z, Huang R, Wu R (2012) Possible linkage between the monsoon trough variability and the tropical cyclone activity over the western North Pacific. Mon Weather Rev 140:140–150. https://doi.org/10.1175/MWR-D-11-00078.1

Wu L, Wen Z, Li T, Huang R (2014) ENSO-phase dependent TD and MRG wave activity in the western North Pacific. Clim Dyn 42:1217–1227. https://doi.org/10.1007/s00382-013-1754-4

Wu L, Wen Z, Wu R (2015) Influence of the monsoon trough on westward-propagating tropical waves over the western North Pacific. Part II: energetics and numerical experiments. J Clim 28:9332–9349. https://doi.org/10.1175/JCLI-D-14-00807.1

Zhan R, Wang Y, Ying M (2012) Seasonal forecasts of tropical cyclone activity over the western North Pacific: a review. Trop Cyclone Res Rev 1:307–324. https://doi.org/10.6057/2012TCRR03.07

Zhang W, Vecchi GA, Murakami H et al (2016) Influences of natural variability and anthropogenic forcing on the extreme 2015 accumulated cyclone energy in the western North Pacific. Bull Amer Meteorol Soc 97:S131–S135. https://doi.org/10.1175/BAMS-D-16-0146.1

Zhao H, Jiang X, Wu L (2015) Modulation of Northwest Pacific tropical cyclone genesis by the intraseasonal variability. J Meteorol Soc Jpn Ser II 93:81–97. https://doi.org/10.2151/jmsj.2015-006

Zhou H, Hsu P-C (2023) Distinct influences of two boreal summer intraseasonal oscillation modes on synoptic-scale eddies over the western North Pacific. Mon Weather Rev 151:953–966. https://doi.org/10.1175/MWR-D-22-0218.1

Zhou H, Hsu P-C, Qian Y (2018) Close linkage between quasi-biweekly oscillation and tropical cyclone intensification over the western North Pacific. Atmos Sci Lett 19:e826. https://doi.org/10.1002/asl.826

Zhou H, Hsu P-C, Chen L, Qian Y (2024) Interannual variability of boreal summer intraseasonal oscillation over the Northwestern Pacific influenced by the Pacific meridional mode. Atmos Ocean Sci Lett https://doi.org/10.1016/j.aosl.2024.100492